# HEAT TRANSFER ENHANCEMENT IN AN INCLINED SOLAR COLLECTOR USING PARTIALLY DRIVEN COLD WALL AND CARBON NANOTUBES BASED NANOFLUID

by

***Chemseddine MAATKI[a], Mohammed A. ALMESHAAL[a], and Lioua KOLSI[b,c*]***

[a]Department of Mechanical Engineering, College of Engineering,
Imam Mohammad Ibn Saud Islamic University, Riyadh, Saudi Arabia
[b]Department of Mechanical Engineering, College of Engineering, Hai'l University,
Hai'l City, Saudi Arabia
[c]Laboratory of Metrology and Energy Systems, National Engineering School,
Energy Engineering Department, University of Monastir, Monastir, Tunisia

Original scientific paper
https://doi.org/10.2298/TSCI220520144M

*In order to improve the performance of a solar collector in low heat transfer rate zones, a 3-D numerical study of the effects of partially moving wall sections and the use of a water nanofluid (CNT) in a tilted parallelepiped solar collector was performed. Equations governing the mixed convection phenomena occurring in the cavity are developed based on the 3-D potential-vorticity formulation and solved using the finite volume method. Two cases related to the direction of the moving surfaces are considered and compared to the base case (no driven walls). The results are presented in term of flow structures, temperature fields and local and average Nusselt numbers. The Richardson number is varied from 0.001 to 10 and the CNT volume fraction from 0 to 0.045. The results showed that for low Richardson values (less than 1), the motion direction of the moving surfaces has no significant effect on heat transfer rates and becomes effective for higher values. The highest rates of heat transfer are found for high Richardson values and CNT volume fractions, while the enhancement ratio (compared to the base case) occurs for low Richardson values.*

Key words: *heat transfer enhancement, partially driven surfaces, nanofluids, 3-D numerical analysis, solar collector*

## Introduction

Industrial applications of movable cover engineering, including manufacturing of solar collectors and heat exchangers, are significantly growing in recent years due to the important enhancement of heat transfer rates induced by such systems. The physical phenomenon generated in such configurations is governed by mixed thermal convection: forced convection and natural convection. Convective heat transfer in lid-driven cavities is the result of association of the motion of the lid causing the shearing flow and natural convection caused

*Corresponding author, e-mail: lioua_enim@yahoo.fr

by the buoyancy forces. Some works have been recently performed on convective heat transfer in lid-driven cavities filled with nanofluids. Tiwari and Das [1] developed a numerical model to analyze the behavior of nanofluids inside heated double lid-driven square cavity. It was observed that Richardson number as well as the direction of the moveable walls changes the flow structure and affects the heat transfer rate. Chamkha and Abu-Nada [2] examined numerically two nanofluid viscosity approximation models (Brinkman model and the Pak and Cho correlation), on the mixed convection in lid-driven square filled with water-$Al_2O_3$ nanofluid. For both models, significant enhancement of heat transfer occurs by using nanofluids especially at high Richardson number values. Muthtamilselvan and Doh [3] studied the mixed convection in a lid-driven square cavity filled with Cu-water nanofluid in the presence of internal heat generation. It was mentioned that the solid volume fraction and Richardson number have significant effects on the flow fields and the heat transfer rate. The 3-D unsteady turbulent mixed convection of four types of nanofluids in a double-lid-driven enclosure under uniform heat flux on the central part of the bottom wall, was investigated by Kareem and Gao [4] using a two-phase mixing model. The author observed that increasing the nanoparticle volume fraction and Reynolds number induces an increase of Nusselt number and flow intensity. Mixed convection of a $Al_2O_3$ nanofluid in a confined lid-driven enclosure having an internal heated square pad in was investigated by Kapil *et al.* [5]. It was concluded that heat transfer rate rises with the concentration of nanoparticles only at high Reynolds number values. The mixed convection heat transfer of Cu-water nanofluid in a double lid-driven cavity with an imposed sinusoidal temperature at the active wall was studied by Reza *et al.* [6] using the Boltzmann lattice method. The authors showed that the average Nusselt number is considerably increased by using both the driven-walls and nanofluid. The mixed convection in a lid-driven trapezoidal cavity heated from the bottom and filled with nanofluids was examined numerically by Kareem *et al.* [7]. The authors studied four different types of nanoparticles ($SiO_2$, $Al_2O_3$, $TiO_2$, and CuO) and showed $SiO_2$-water nanofluid provides the highest Nusselt number values. Mirzakhanlari *et al.* [8] conducted a 2-D numerical study on the mixed convection in a lid-driven cavity filled with $Al_2O_3$ nanofluid equipped with an internal rotating cylinder. The authors revealed that the Nusselt average and drag coefficient increase with Richardson number and nanoparticles concentration. The mixed convection in a double-lid-driven cubic cavity having multiple heating sources and filled with $Al_2O_3$-water was studied numerically by Zhou *et al.* [9]. The authors found that the driven walls cause a considerable enhancement of the heat transfer. A similar study was conducted by Xia *et al.* [10] in a *T*-shaped cavity. Hatami *et al.* [11] studied the mixed convection in a porous cavity saturated with various nanofluids ($Al_2O_3$, Cu, and $TiO_2$). They proved that the use of nanofluids significantly enhances the heat transfer rate. The entropy generation by the mixed convection in a lid-driven cavity filled with $Al_2O_3$-filled was investigated by Gibanov *et al.* [12]. The authors mentioned that the increase of nanoparticles volume fraction leads to an enhancement of the heat transfer rate and the decrease of the average Bejan number. Cho [13] conducted a numerical investigation on the heat transfer and entropy generation during mixed convective flow in a corrugated lid-driven cavity filled with Cu-water nanofluid. He showed that the average Nusselt number and the total entropy generation rise with the Richardson number, the volume fraction of the nanoparticles, and the Reynolds number. He also found that the total entropy generation and the average Nusselt number increase with the amplitude of the corrugated surface. Selimefendigil [14] studied the mixed convection in a lid-driven cavity having an elliptical inner obstacle and filled with single and multiple wall carbon nanotubes. The author showed the presence of an optimal size of the inner obstacle allowing a maximum average heat transfer rate. He also mentioned that the average heat transfer rate increases by more than 120% for a volume fraction of 0.06. several interesting works related to the subject can be found in the literature [15-24].

The objective of the present work is to study numerically a new design based on a partially lid driven cavity with the aim to improve the heat transfer rate in a 45° inclined differentially heated cavity assimilated to a solar collector. The driven parts are limited to the top and bottom of the cold wall, the aim of this choice is to enhance the heat transfer in these zones while avoiding the important amount of energy required to drive all the wall. In fact, analysis of the flow structure and pure natural convection heat transfer rates in a rectangular solar collector shows that the velocity field in the top and bottom regions is damped due to boundary layer effects. This causes the decrease of the flow intensity and leads to a decrease in local heat transfer rates. The novelty of this work is to improve the heat transfer rate in these zones inducing subsequently an improvement of the global heat transfer rates in the solar collector. The proposed solution consists of using partial mechanically moving parts of the cold wall in addition to the use of the CNT-nanofluid as working fluid.

## Studied configuration and mathematical formulation

### *Physical model*

The studied configuration, fig. 1, corresponds to a high and tilted solar collector with aspect ratios of 5 and 10 along the z and y directions, respectively.

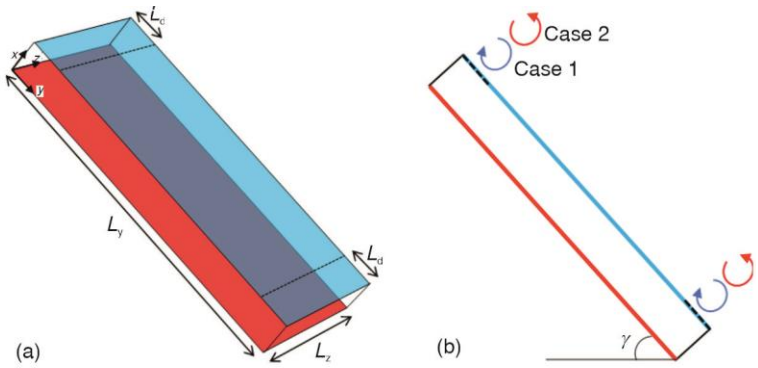


**Figure 1. Physical model; (a) 3-D configuration and (b) the XY-central plan**

The cavity of the solar collector is filled with CNT-water nanofluid and is subjected to temperature gradient, such that the bottom surface is hot and the top is cold. The system of moving walls of dimension $L_\mathrm{d}$ (in the $y$-direction), placed respectively at the top and bottom of the cavity is modeled by two surfaces located at the top and bottom of the cold wall moving towards the $y$-axis. Only these surfaces of dimension, $L_\mathrm{d} \times L_x$, are considered movable. Two cases (Cases 1 and 2), corresponding to the direction of the velocity of the driven surfaces, are studied and compared to the basic case (Case 0) where the surfaces are kept motionless.

### *Mathematical formulation*

The fluid is supposed being Newtonian and incompressible. The flow is considered to be laminar. The Boussinesq approximation is used to approximate the density of the fluid.

All other thermophysical properties of the fluid are considered as constant. Governing equations for the solar collector model under investigation are then written using the 3-D potential-vorticity vector formulation $(\vec{\psi} - \vec{\omega})$ which de-emphasizes the pressure gradient. The stated governing equations are then provided in dimensionless form:

$$-\vec{\omega} = \nabla^2 \vec{\psi} \tag{1}$$

$$\frac{\partial \vec{\omega}}{\partial t} + (\vec{u}\nabla)\vec{\omega} - \frac{\nu_{\mathrm{nf}}}{\nu_{\mathrm{f}}} \Pr(\vec{\omega}\nabla)\vec{u} = \Delta\vec{\omega} + \frac{\beta_{\mathrm{nf}}}{\beta_{\mathrm{f}}} \mathrm{Ra}\Pr \begin{bmatrix} \left(\dfrac{\partial T}{\partial z}\right)\cos\gamma \\ \left(-\dfrac{\partial T}{\partial z}\right)\sin\gamma \\ \left(-\dfrac{\partial T}{\partial x}\cos\gamma + \dfrac{\partial T}{\partial y}\sin\gamma\right) \end{bmatrix} \tag{2}$$

$$\frac{\partial T}{\partial t} + \vec{u}\nabla T = \frac{\alpha_{\mathrm{nf}}}{\alpha_{\mathrm{f}}} \nabla^2 T \tag{3}$$

with

$$\mathrm{Ra} = \frac{\mathrm{g}\beta_T (T_h - T_C) L^3}{\nu\alpha}, \quad \Pr = \frac{\nu}{\alpha} \tag{4}$$

The set of governing equations is discretized and solved via the control volume method using central difference scheme. The convergence criterion is:

$$\sum_{i}^{1,2,3} \frac{\max\left|\psi_i^n - \psi_i^{n-1}\right|}{\max\left|\psi_i^n\right|} + \max\left|T_i^n - T_i^{n-1}\right| \le 10^{-5} \tag{5}$$

The boundary conditions of the studied model are:

Temperature

$$\text{At } x = 0, T = 1 \text{ (hot wall) and } T = 0 \text{ for } x = 1 \text{ (cold wall)} \tag{6}$$

$$\text{On all the adiabatic walls, } \frac{\partial T}{\partial n} = 0 \tag{7}$$

Vorticity

$$\omega_x = 0,\ \omega_y = -\frac{\partial u_3}{\partial x},\ \omega_z = \frac{\partial u_2}{\partial x} \text{ at } x = 0 \text{ and } x = 1 \tag{8}$$

$$\omega_x = \frac{\partial u_3}{\partial y},\ \omega_y = 0,\ \omega_z = -\frac{\partial u_1}{\partial y} \text{ at } y = 0 \text{ and } y = 1 \tag{9}$$

$$\omega_x = -\frac{\partial u_2}{\partial z},\ \omega_y = -\frac{\partial u_1}{\partial z},\ \omega_z = 0 \text{ at } z = 0 \text{ and } z = 1 \tag{10}$$

Vector potential

$$\frac{\partial \psi_x}{\partial x} = \psi_y = \psi_z = 0 \text{ at } x = 0 \text{ and } x = 1 \tag{11}$$

$$\psi_x = \frac{\partial \psi_y}{\partial y} = \psi_z = 0 \text{ at } y = 0 \text{ and } y = 1 \tag{12}$$

$$\psi_x = \psi_y = \frac{\partial \psi_z}{\partial z} = 0 \text{ at } z = 0 \text{ and } z = 1 \tag{13}$$

Velocity

$$u_1 = u_2 = u_3 = 0 \text{ at } x = 0 \text{ and } 1 \le y \le 9 \tag{14}$$

$$u_1 = u_2 = u_3 = 0 \text{ at } z = 0 \text{ and } z = 1 \tag{15}$$

$$u_2 = \pm \frac{\rho_{\mathrm{nf}} c_{p,\mathrm{nf}} k_{\mathrm{f}}}{\rho_{\mathrm{f}} c_{p,\mathrm{f}} k_{\mathrm{nf}}} \mathrm{Re}\,\mathrm{Pr} \text{ at } x = 1,\ 0 \le y \le 1 \text{ and } 9 \le y \le 10 \text{ (driven parts)} \tag{16}$$

The Richardson number is defined as:

$$\mathrm{Ri} = \frac{\mathrm{Gr}}{\mathrm{Re}^2} = \frac{\mathrm{Ra}}{\mathrm{Pr}\mathrm{Re}^2} \tag{17}$$

The local and average Nusselt are provided:

$$\mathrm{Nu} = \left(\frac{k_{\mathrm{nf}}}{k_{\mathrm{f}}}\right) \frac{\partial T}{\partial x}\bigg|_{x=0,1}, \quad \mathrm{Nu}_{\mathrm{av}} = \int_0^1 \int_0^1 \mathrm{Nu}\,\partial y \partial z \tag{18}$$

The ratio $\mathrm{Nu}_{\mathrm{av}}/\mathrm{Nu}_{\mathrm{Re0}}$ called as enhancement ratio, is the ratio between the average Nusselt numbers in Cases 1 and 2 to the average Nusselt numbers in Case 0.

The following expressions are used to evaluate the effective properties of the nanofluid:

$$\rho_{\mathrm{nf}} = (1-\phi)\rho_{\mathrm{f}} + \phi\rho_{\mathrm{s}} \tag{19}$$

$$c_{p,\mathrm{nf}} = \frac{(1-\phi)(\rho_{\mathrm{f}}\, c_{p,\mathrm{f}}) + \phi(\rho_{\mathrm{CNT}}\, c_{p,\mathrm{CNT}})}{\rho_{\mathrm{nf}}} \tag{20}$$

$$\beta_{\mathrm{nf}} = \frac{(1-\phi)(\rho_{\mathrm{f}}\, \beta_{\mathrm{f}}) + \phi(\rho_{\mathrm{CNT}}\, \beta_{\mathrm{CNT}})}{\rho_{\mathrm{nf}}} \tag{21}$$

$$\mu_{\mathrm{nf}} = \mu_{\mathrm{f}}\left(1 + a\phi + b\phi^2\right) \tag{22}$$

where $a$ = 13.5 and $b$ = 904.4 for tube shaped nanoparticles (Hamilton and Crosser model):

$$k_{\mathrm{nf}} = k_{\mathrm{f}} \frac{(1-\phi) + 2\phi \dfrac{k_{\mathrm{CNT}}}{k_{\mathrm{CNT}} - k_{\mathrm{f}}} \ln \dfrac{k_{\mathrm{CNT}} + k_{\mathrm{f}}}{2k_{\mathrm{f}}}}{(1-\phi) + 2\phi \dfrac{k_{\mathrm{f}}}{k_{\mathrm{CNT}} - k_{\mathrm{f}}} \ln \dfrac{k_{\mathrm{CNT}} + k_{\mathrm{f}}}{2k_{\mathrm{f}}}} \tag{23}$$

## Validation of the code and grid independency test

### *Validation of the numerical code*

To check the validity of the current numerical code, a qualitative comparison of the flow structure with the experimental findings of Leporini *et al.* [26] who studied the 3-D natural convection, is performed, fig. 2. Then a quantitative verification for the case of 3-D lid-driven cavity filled with a nanofluid is performed by comparing with the recently published numerical results of Ghasemi and Siavashi [27], fig. 3. The comparisons show a good agreement with the results presented in the literature. Table 1 shows the properties of water and CNTs fluid [25]

**Table 1. Properties of CNT and water [25]**

| Physical properties | Water | CNTs |
|---|---|---|
| ρ (kg.m-3) | 997.1 | 2600 |
| CP (J.kg-1.K-1) | 4179 | 425 |
| μ (Pa.s) | 10-3 | -- |
| k (W.m-1. K-1) | 0.613 | 6600 |
| β (K-1) | $2.1\ 10^{-6}$ | $16\ 10^{-7}$ |

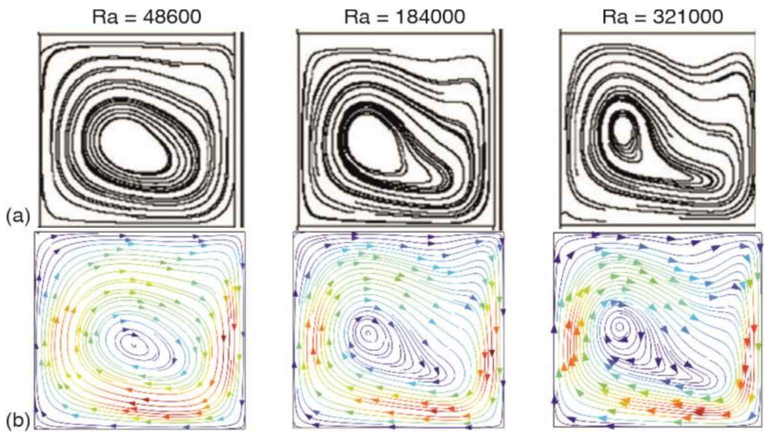


**Figure 2. Validation of the present numerical model with the experimental results of Leporini *et al.* [26] (a) and present code (b)**

*Grid independency test*

The accuracy of the results is checked in tab. 2 by performing a grid independency test based on the comparison of the results of the average Nusselt number for four grids. The average Nusselt number is chosen as sensitive variable and the deviation between its values for G3 and G4 is less than 0.3%. Thus, for time economy and results accuracy the grid G3 (25×125×250) is retained for all the performed simulations.

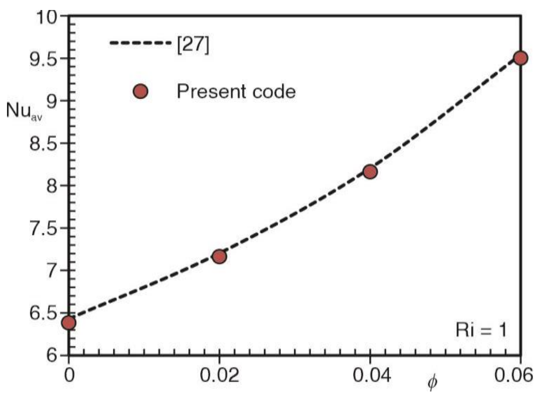


**Figure 3. Verification of the numerical code with the numerical results of Ghasemi and Siavashi [27] for the case of a 3-D lid-driven nanofluid-filled cavity**

## Results and discussion

A numerical study on the mixed natural convection in a rectangular parallelepiped inclined cavity is investigated. The cavi-

**Table 2. Grid sensitivity for case 1 (Ri = 1 and $\phi$ = 0.045)**

| | Grid | $Nu_{avg}$ | Percentage Increase | Incremental Increase |
|---|---|---|---|---|
| G1 | 15×150×75 | 4.1588 | – | – |
| G2 | 20×200×100 | 4.2351 | 1.834664 | – |
| G3 | 25×125×250 | 4.377 | 5.246706 | 3.35057 |
| G4 | 30×150×300 | 4.3894 | 5.544869 | 0.283299 |

ty is differentially heated, filled with CNT/water-nanofluid and equipped by two moving surfaces located at the bottom and top of the cold wall. Three different cases are studied; Case 0 (reference), corresponds to pure natural convection (no driven walls); case 1 corresponds to moving surfaces having upward velocities and Case 2 is when the velocities of moving surfaces are downward. The numerical simulations are performed for a Richardson number varying between 0.001 and 10 and CNT volume fraction varying between 0% and 4.5%. Qualitative results are presented in terms of temperature fields, flow structures, and local Nusselt number iso-contours, and quantitative results are displayed in term of average values of Nusselt number.

### *Flow structure analysis*

Figure 4 shows the 3-D flow structures for the three considered cases for a CNT volume fraction of 4.5%. Case 0 is the base case where the flow induced only by thermal

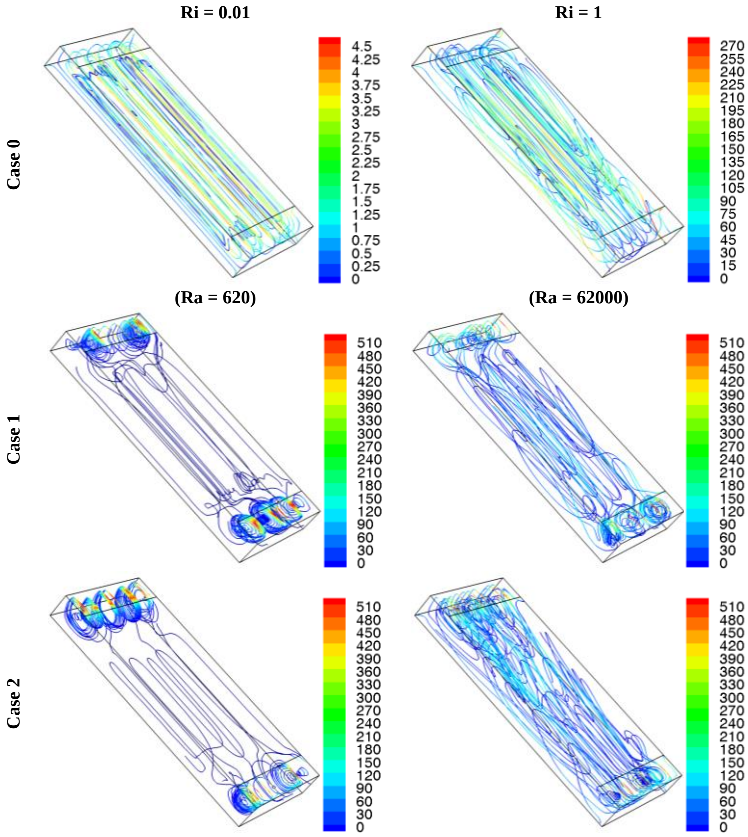


**Figure 4. Particles' trajectories for the considered cases for $\phi$ = 0.045**

buoyancy forces. For Ra = 620, the flow velocity is weak, characterized by a rough motion of the fluid with an ascending motion close to hot wall and descending close to the cold wall. The increase of Rayleigh number leads to a significant increase of the flow velocity. The flow structure in this case is similar to the results of Tiwari and Das [1] when the natural convection regime was dominant. Case 1 is defined by an upward moving of the two driven surfaces. The driving forces induced by the movement of the moving surfaces are in this case opposed to the thermal volume forces leading to a stabilization of the flow and very low velocities occur at the central region of the cavity for Ri = 0.01. For Ri = 1, the impact of the buoyancy forces becomes more intense. Thus, the flow intensity increases in the central region. The three-dimensional character of the flow becomes more pronounced, and three flow zones are identified separately in the cavity. Two zones are at the top and bottom of the cavity and are governed by forced convection effects of due to the moving walls and a central zone driven by natural convection effects generated by the thermal volume forces.

Case 2 is characterized by a decreasing velocity (upper to down) of the moving surfaces located at the bottom and at the top of the cold wall. The maximum velocity of the fluid is doubled compared to reference case (Case 0). For Ri = 0.01, the flow becomes characterized by rotating vortexes located near the moving surfaces. The flow in core region of the cavity is relatively weak. The movements of the two moving surfaces tend to favour the downward fluid motion and co-operates with the thermal buoyancy forces. The strength of the induced vortexes in these zones is explained by the weakness of the thermal volume forces compared to the effect of the moving surfaces. For Ri = 1, the intensity of the vortexes is reduced since thermal volume forces become more important and drive the fluid flow along the whole cavity. For Ri = 1, a competition between the driving forces induced by the motion of the moving surfaces and the buoyancy forces is observed in both Cases 1 and 2. This competition leads to a complex 3-D flow as stated in the work of Ghachem *et al.* [28]. In order to

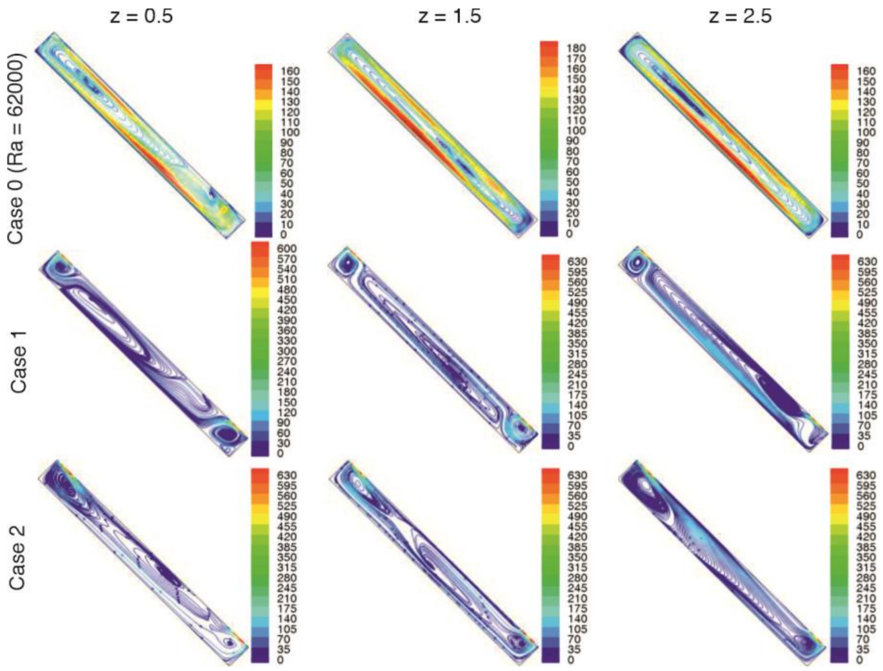


**Figure 5. Flow patterns at different z-plans for $\phi$ = 0.045 and Ri = 1**

illustrate the occurrence of this three-dimensional flow character at this Richardson number, the flow structures in different constant z-plans ($z$ = 0.5, $z$ = 1.5 and $z$ = 2.5 (central plan)) are plotted in fig. 5. For Case 0, the flow structures at $z$ = 0.5 and $z$ = 2.5 plans show that the thermal vortex is located in the upper part of the cavity, while it is located in the lower part for $z$ = 1.5 plan. The boundary-layer effect due to viscous friction near the adiabatic walls is observed in the lower part of the cavity at $z$ = 0.5 plan. At the central plan, the maximum velocity is observed near the two active walls, while in the other two plans it is mainly observed near the hot wall. For Case 1, the flow structures at $z$ = 0.5 and $z$ =1.5 plans are characterized by three counter-rotating vortexes. Two counter-clockwise vortexes are situated at the top and bottom of the cavity and are caused by the shear forces generated by the moving surfaces effect. The third vortex is driven by thermal volume forces and is located at the upper zone of the cavity at the plan $z$ = 0.5 and in the central zone for the plan $z$ = 1.5. The flow structure at the central plan ($z$ = 2.5), is characterized by only two counter-rotating vortexes. The vortex located at the top of the cavity persists while the clockwise vortex situated at the bottom of the cavity is merged with the central vortex to form a larger vortex stuck to the cold wall and situated in the lower region of the cavity. This fact indicates that the forced convection is dominant compared to natural convection.

For Case 2, the moving surfaces have a downward velocity. In this case, the shear forces generated by the motion of the moving surfaces, act in the same direction as the buoyancy forces. The flow structure in the secondary plans $z$ = 0.5 and $z$ = 1.5 is characterized by three clockwise vortexes, situated at the top, in the middle and at the bottom of the cavity. While in the central plan $z$ = 2.5, the flow structure is characterized by two vortexes, located at the top and bottom of the cavity. The vortex located at the top of the cavity is a result of the coalescence between the vortex due to volume forces and the vortex due to shear forces.

## *Heat transfer characterization*

### *Iso-temperatures pattern*

The analysis of the iso-temperature pattern provides a characterization of the heat transfer in the cavity. Figure 6 shows the temperature iso-contours in the central plan of the cavity ($z$ = 2.5) for the three considered cases under different Richardson numbers. For the reference case, at Ra = 620, the isotherms are stratified close to the active walls indicating the dominance of conductive regime. For Ra = 62000 and Ra = 620000, *S*-shaped distortions are observed indicating the dominance of the convective regime. The thermal gradient is strong at the bottom of the cavity near the hot wall and weak at the top. On the other hand, it is weak at the bottom and strong at the top of the cavity near the cold wall.

For Case 1, when Ri = 0.01, the temperature iso-contours show a mainly conductive regime located in the central zone of the cavity, while it shows deformations near the moving surfaces indicating the dominance of convection. For Ri = 1 and 10, the temperature iso-contours reveal an increase of the thermal gradients at the top of the hot wall compared to Case 0. For Case 2, and for Richardson number values of 1 and 10, thermal gradients become strong along the entire length of both the hot and cold wall, because of the mixed convection effects.

### *Local Nusselt distribution*

By analyzing previous research works, we noticed that the results of three-dimensional mixed convection studies presented in the literature do not highlight the Richardson effect and the presence of nanoparticles on the local Nusselt distribution. As the novelty is based on the enhancement of the heat transfer rate in the areas near the upper and lower side walls of the cavity. Figure 7 depicts the local Nusselt patterns at the hot wall for the three studied cases for Ri = 0.1 and $\phi = 0$ and 0.045. For the three examined cases, an improvement of the heat transfer rate is observed with the addition of nanoparticles. On the other hand, a 3-D effect, reflected by a variation in the *z*-direction, is noticed in the local Nusselt distribution. For Case 0, the maximum heat transfer rate is found in the lower zone of the hot wall. In addition, three vertically alternating zones in the central part of the hot wall exhibit relatively high local Nusselt values. For Case 1, the local heat transfer rate is improved compared to Case 0. In fact, the local Nusselt number is relatively enhanced at the top of the hot wall. The local Nusselt distribution in the lower part of the wall exhibits a slight upward shift compared to Case 0 due to the upward movement of the lower moving surface. The local Nusselt distribution for Case 2, is characterized by a higher improvement compared to Cases 0 and 1. Furthermore, the local Nusselt maximum at the top of the wall is found in three cells revealing the impact of the three-dimensional character of the flow.

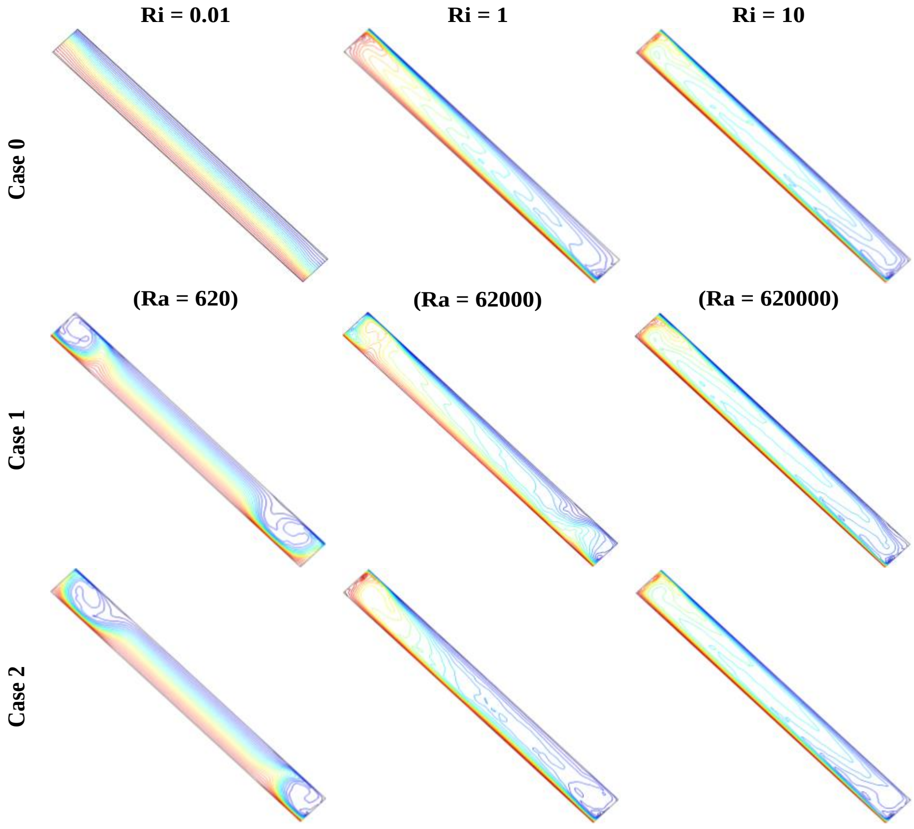


**Figure 6. Effect of Richardson number on isotherms at *z* =2.5 plan for $\phi$ = 0.045**

### *Effect of Richardson number and CNT volume fraction on average heat transfer rate*

The effect of Richardson number on the average heat transfer for Cases 1 and 2 is illustrated in fig. 8(a). The increase of Richardson number improves the average heat transfer rate. The same result was observed in references [13-15]. In fact, the increase of Richardson

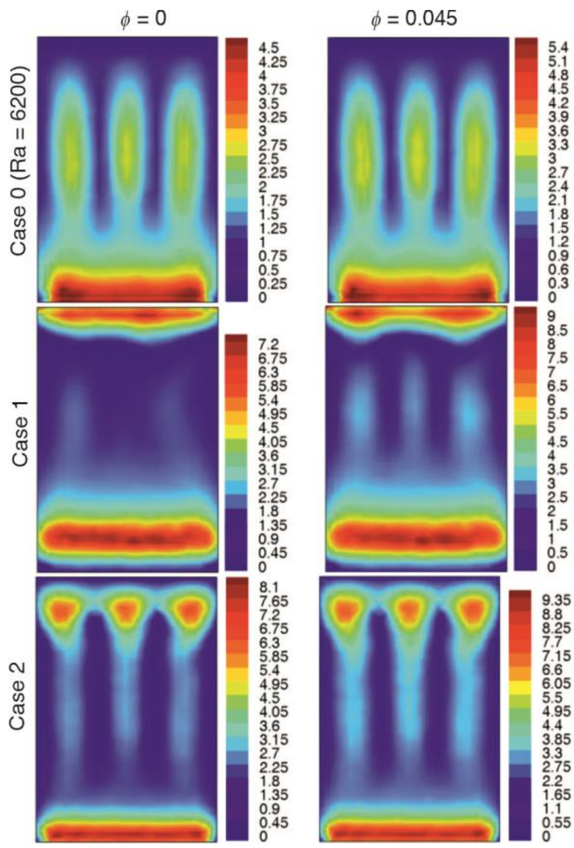

**Figure 7. Local Nusselt pattern at hot wall for Ri=0.1, $\phi$ = 0 and $\phi$ = 0.045**

number from 0.01 to Ri = 0.1 leads to a 20% improvement in the average heat transfer rate. The variation of the average Nusselt number *vs*. Richardson number follows an exponential profile, with an improvement reaching 200% for Ri = 10. For low Richardson number values, the average Nusselt number values are equal for Cases 1 and 2, indicating that the effect of the direction of the driven surfaces is unsignificant on the heat transfer rate. For Ri ≥ 1 the heat transfer rate is more important for Case 2 compared to Case 1. Figure 8(b) presents the effect of nanoparticles volume fraction on the heat transfer rate for Cases 1 and 2. Increasing the nanoparticles volume fraction enhances the heat transfer rate for the two cases. Mirzakhanlari *et al.* [8] also showed that the Nusselt mean with Richardson number and nanoparticle concentration. The trend of the average Nusselt *vs*. the nanoparticles volume fraction is quasi-linear. The normalized heat transfer rate in the ratio of the average Nusselt numbers of the specific Cases 1 or 2 by the reference Case 0. Figure 9 shows the effect of Richardson and nanoparticles volume fraction on this ratio. Figure 9(a) displays the effect of Richardson number on the normalized heat transfer. The maximum enhancement is observed for low Richardson number values, and it is higher for Case 1 than Case 2. For higher Richardson values, the normalized heat transfer decreases progressively and becomes more important for Case 2 compared to Case 1. Figure 9(b) shows the effect of nanoparticles volume fraction on the normalized heat transfer rate for Ri = 0.01 and 10. For Case 1, the normalized heat transfer is quasi-constant *vs*. the nanoparticles volume fraction. While a slight increase occurs for Case 2, that reaches 6% for $\phi$ = 4.5%.

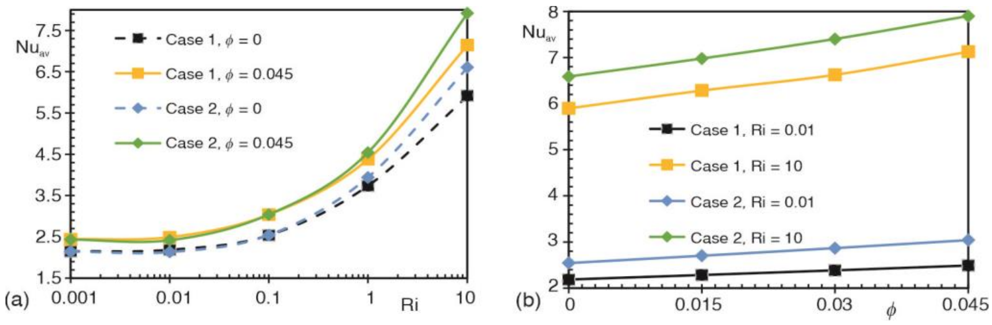


**Figure 8. Effect of Richardson number (a) and nanoparticles volume fraction (b) on Nu$_{av}$**

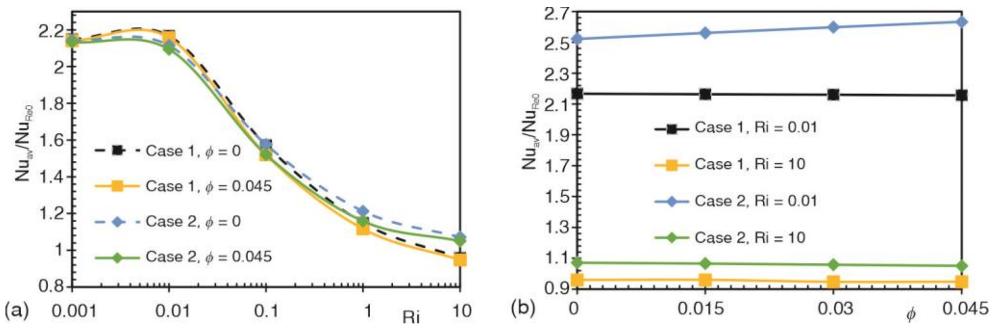


**Figure 9. Effect of Richardson number (a) and nanoparticles' fraction volume (b) on the normalized heat transfer rate**

## Conclusion

This work provides a 3-D numerical study on the mixed thermal convection in a solar collector, modeled as an inclined parallelepiped cavity filled with a CNT-nanofluid. The active cold wall is partially driven at the top and bottom parts to cause better heat transfer in these regions where the flow intensity is basically relatively low. The governing equation are developed using the vorticity vector potential formulation and discretized using the finite volume method. The effects of the direction of the moving surfaces, Richardson number, and the CNT volume fraction are studied and discussed. It was found that the effect of the driven surfaces on the flow structure and temperature field becomes tangible for higher values of Richardson number especially for Case 2. Compared to the base case the use of partially driven surfaces enhances the local heat transfer at the top and bottom regions and consequently leads to the improvement of the overall heat transfer rate. The use of the CNT gives an additional boost to the heat transfer by improving the thermophysical properties of the working fluid. As extension of the present work, it planned to study the effects of the inclination, the addition of fins and the use of hybrid nanofluids.

## Acknowledgment

This research was funded by the Deanship of Scientific Research, Imam Mohammad Ibn Saud Islamic University, Saudi Arabia, Grant No. (20-13-14-002).

## Nomenclature

$c_p$ – specific heat capacity, [kJkg$^{-1}$K$^{-1}$]
g – gravitational acceleration, [ms$^{-2}$]
$k$ – thermal conductivity, [kWm$^{-1}$K$^{-1}$]
$L_d$ – length of the driven section
Nu – Nusselt number
Pr – Prandtl number
Ra – Rayleigh number
Ri – Rishardson number
Gr – Grashof number
$T$ – dimensionless temperature
$t$ – dimensionless time
$\vec{u}$ – dimensionless velocity vector
$x,y,z$ – dimensionless cartesian co-ordinates

*Greek symbols*

$\alpha$ – thermal diffusivity, [m$^2$s$^{-1}$]
$\beta$ – thermal expansion coefficient, [K$^{-1}$]
$\gamma$ – cavity inclination
$\mu$ – dynamic viscosity, [Pa.s]
$\nu$ – kinematic viscosity, [m$^2$s$^{-1}$]
$\rho$ – density of the fluid, [kgm$^{-3}$]
$\phi$ – nanoparticles volume fraction
$\vec{\psi}$ – dimensionless Vector potential
$\vec{\omega}$ – dimensionless vorticity

*Subscripts*

av – average
c – cold

f – fluid
h – hot
nf – nanofluid

## References


[1] Tiwari, R., Das, M. K., Heat Transfer Augmentation in a Two-Sided Lid-Driven Differentially Heated Square Cavity Utilizing Nanofluids, *International Journal of Heat and Mass Transfer, 50* (2007), 9-10, pp. 2002-2018

[2] Chamkha, A. J., Abu-Nada, E., Mixed Convection Flow in Single- and Double-Lid Driven Square Cavities Filled with Water-$Al_2O_3$ Nanofluid: Effect of Viscosity Models, *European Journal of Mechanics - B/Fluids, 36* (2012), Nov.-Dec., pp. 82-96

[3] Muthtamilselvan, M., Doh, D. H., Mixed Convection of Heat Generating Nanofluid in a Lid-Driven Cavity with Uniform and Non-Uniform Heating of Bottom Wall, *Applied Mathematical Modelling, 38* (2014), 13, pp. 3164-3174

[4] Kareem, A., Gao, S., Computational Study of Unsteady Mixed Convection Heat Transfer of Nanofluids in a 3D Closed Lid-Driven Cavity, *International Communications in Heat and Mass Transfer, 82* (2017), Mar., pp. 125-138

[5] Kapil, M., *et al.*, A Numerical Study of 2-D Convective Heat Transfer of Nanofluid (Al2O3/H2O) in a Lid Driven Cavity with Square Cylinder at the Centre, *Materials Today: Proceedings, 11* (2019), 2, pp. 700-707

[6] Reza, A., *et al.*, Numerical Simulation of Mixed Convection Heat Transfer of Nanofluid in a Double Lid-Driven Cavity Using Lattice Boltzmann Method, *Alexandria Engineering Journal, 55* (2016), 4, pp. 3101-3114

[7] Kareem, A. K., *Et Al.*, Numerical Investigation Of Mixed convection heat transfer of Nanofluids in a Lid-Driven Trapezoidal Cavity, *International Communications in Heat and Mass Transfer, 77* (2016), Oct., pp. 195-205

[8] Mirzakhanlari, S., *et al.*, Increment of Mixed Convection Heat Transfer and Decrement of Drag Coefficient in a Lid-Driven Nanofluid-Filled Cavity with a Conductive Rotating Circular Cylinder at Different Horizontal Locations: A Sensitivity Analysis, *Powder Tech., 305* (2017), Jan., pp. 495-508

[9] Zhou, W., *et al.*, Lattice Boltzmann Simulation of Mixed Convection of Nanofluid with Different Heat Sources in a Double Lid-Driven Cavity, *International Communications in Heat and Mass Transfer, 97* (2018), Oct., pp. 39-46

[10] Xia, S., *et al.*, Numerical Investigation of Nanofluid Mixed Convection in a T-Shaped Cavity by Considering a Thermal Barrier, *Alexandria Engineering Journal, 61* (2022), 9, pp. 7393-7415

[11] Hatami, M., *et al.*, Optimization of a Lid-Driven T-Shaped Porous Cavity to Improve the Nanofluids Mixed Convection Heat Transfer, *Journal of Molecular Liquids, Volume 231* (2017), Apr., pp. 620-63

[12] Cho, C. C., Heat Transfer and Entropy Generation of Mixed Convection Flow in Cu-Water Nanofluid-Filled Lid-Driven Cavity with Wavy Surface, *International Journal of Heat and Mass Transfer, 119* (2018), Apr., pp. 163-174

[13] Gibanov, N. S., *et al.*, Mixed Convection with Entropy Generation of Nanofluid in a Lid-Driven Cavity Under the Effects of a Heat-Conducting Solid Wall and Vertical Temperature Gradient, *European Journal of Mechanics - B/Fluids, 70* (2018), July-Aug., pp. 148-159

[14] Selimefendigil, F., Mixed Convection in a Lid-Driven Cavity Filled with Single and Multiple-Walled Carbon Nanotubes Nanofluid Having an Inner Elliptic Obstacle, *Propulsion and Power Research, 8* (2019), 2, pp. 128-137

[15] Li, Z., *et al.*, Mixed Convection of Non-Newtonian Nanofluid in an H-Shaped Cavity with Cooler and Heater Cylinders Filled by a Porous Material: Two Phase Approach, *Advanced Powder Technology, 30* (2019), 11, pp. 2666-2685

[16] Kavusi, H., Toghraie, D., A Comprehensive Study of the Performance of a Heat Pipe by Using of Various Nanofluids, *Advanced Powder Technology, 28* (2017), 11, pp. 3074-3084

[17] Ruhani, B., *et al.*, Statistical Investigation for Developing a New Model for Rheological Behavior of Silica-Ethylene Glycol/Water Hybrid Newtonian Nanofluid Using Experimental Data, *Physica A: Statistical Mechanics and its Applications, 525* (2019), July, pp. 616-627

[18] Arasteh, H., *et al.*, Heat and Fluid Flow Analysis of Metal Foam Embedded in a Double-Layered Sinusoidal Heat Sink Under Local Thermal Non-Equilibrium Condition Using Nanofluid, *Journal of Thermal Analysis and Calorimetry, 138* (2019), Mar., pp. 1461-1476

[19] Bazdar, H., *et al.*, Numerical Investigation of Turbulent Flow and Heat Transfer of Nanofluid Inside a Wavy Microchannel with Different Wavelengths, *Journal of Thermal Analysis and Calorimetry, 139* (2020), Aug., pp. 2365-2380

[20] Shaker, B., *et al.*, CFD Analysis of $Al_2O_3$-Syltherm Oil Nanofluid on Parabolic Trough Solar Collector with a New Flange-Shaped Turbulator Model, *Theoretical and Applied Mechanics Letters, 12* (2022), 2, 100323

[21] Sani, F. H., *et al.*, The Effect of $MoS_2$–Ag/ $H_2O$ Hybrid Nanofluid on Improving the Performance of a Solar Collector by Placing Wavy Strips in the Absorber Tube, *Case Studies in Thermal Engineering, 30* (2022), 101760

[22] Gholinia, M., *et al.*, Employing a New Micro-Spray Model and (MWCNTs-SWCNTs)-$H_2O$ Nanofluid on Si-IGBT Power Module for Energy Storage: A Numerical Simulation, *Energy Reports, 7* (2021), Nov., pp. 6844-6853

[23] Ghobadi, A. H., *et al.*, A New Thermal Conductivity Model of CNTs/$C_2H_6O_2$-$H_2O$ Hybrid Base Nanoliquid Between Two Stretchable Rotating Discs with Joule Heating, *International Journal of Ambient Energy, 43* (2022), 1, pp. 3310-3321

[24] Ghobadi, A. H., Hassankolaei, M. G., A Numerical Approach for MHD $Al_2O_3$-$TiO_2$/$H_2O$ Hybrid Nanofluids Over a Stretching Cylinder Under the Impact of Shape Factor, *Heat Transfer, 48* (2019), 8, pp. 4262-4282

[25] Aich, W., *et al.*, Numerical Simulation of Buoyancy-Induced Heat Transfer and Entropy Generation in 3D C-Shaped Cavity Filled with CNT-$Al_2O_3$/Water Hybrid Nanofluid, *International Journal of Nonlinear Sciences and Numerical Simulation*, On-line first, https://doi.org/https://doi.org/10.1515/ijnsns-2021-0246, 2022

[26] Leporini, M., *et al.*, Experimental and Numerical Investigation of Natural Convection in Tilted Square Cavity Filled with Air, *Experimental Thermal and Fluid Science, 99* (2018), Dec., pp. 572-583

[27] Ghasemi, K., Siavashi, M., Three-Dimensional Analysis of Magnetohydrodynamic Transverse Mixed Convection of Nanofluid Inside a Lid-Driven Enclosure Using MRT-LBM, *International Journal of Mechanical Sciences, 165* (2020), 105199

[28] Ghachem, K., *et al.*, Numerical Simulation of Three-Dimensional Double Diffusive Convection in a Lid-Driven Cavity, *International Journal of Thermal Sciences, 110* (2016), Dec., pp. 241-250

Paper submitted: May 20, 2022
Paper revised: August 14, 2022
Paper accepted: August 25, 2022